Journal of Advanced Ceramics
2018, **7**(4): 380–387
https://doi.org/10.1007/s40145-018-0294-0
ISSN 2226-4108
CN 10-1154/TQ

Research Article

Effect of Al_2O_3 addition on the non-isothermal crystallization kinetics and long-term stability of BCABS sealing glass for IT-SOFCs

Zuzhi HUANG[a,b], Linghong LUO[a,b,*], Liangguang LIU[a,b], Leying WANG[a,b,*], Liang CHENG[a], Xu XU[a,b], Yefan WU[a]

[a]*Key Laboratory of Fuel Cell Materials and Devices*, *Jingdezhen Ceramic Institute*, *Jingdezhen 333403*, *China*
[b]*School of Materials Science and Engineering*, *Jingdezhen Ceramic Institute*, *Jingdezhen 333403*, *China*

Received: April 27, 2018; Revised: July 28, 2018; Accepted: August 9, 2018
© The Author(s) 2018. This article is published with open access at Springerlink.com

Abstract: Owing to adjustable thermal expansion performance, $BaO–CaO–Al_2O_3–B_2O_3–SiO_2$ (BCABS) glass has a promising commercialization prospect for intermediate temperature-solid oxide fuel cells (IT-SOFCs) sealing. Herein, Al_2O_3 with two different contents was added into the same glass formulation, referred to as A and B glass, respectively. In terms of the non-isothermal crystallization kinetic behavior, the effect of Al_2O_3 as the unique intermediate was innovatively studied on the long-term performance of BCABS sealing glass. After the heat treatment at 1023 K for 100 h, the change of the network structure and the expansion coefficient of the glass were characterized. The results showed that the addition of Al_2O_3 as a network forming body could enhance the structure of glass, and increase the activation energy for glass transition, which could effectively inhibit the crystallization ability of sealing glass. Therefore, the B glass with the higher Al_2O_3 content showed the better long-term sealing ability, which was greatly beneficial for IT-SOFCs sealing.

Keywords: intermediate temperature-solid oxide fuel cell (IT-SOFC); $BaO–CaO–Al_2O_3–B_2O_3–SiO_2$ (BCABS) sealing glass; Al_2O_3; non-isothermal crystallization kinetics; long-term stability

1 Introduction

Intermediate temperature-solid oxide fuel cells (IT-SOFCs) as electrochemical devices have great potentials in the stationary and mobile applications due to the high-efficiency system of power generation [1,2]. IT-SOFCs could obtain the higher power density by electrochemical reactions, which directly convert hydrogen or hydrocarbon into electricity without any moving parts at the temperature range of 600–800 ℃ [3]. According to the stacking design and fabrication, the planar type and sealless tubular design for IT-SOFCs have been given much favor by researchers at present [4]. The sealless tubular design has a relatively long current path through the cell, which would result in the great resistive loss. As compared to the tubular design, the planar-type IT-SOFCs could provide the higher power density due to the effective planar structure that consists of the repeated unit by the combination of anode–electrolyte–cathode structure and interconnector [5]. The suitable sealing materials must be required to prevent fuel leakage and air mixing at the high operating temperature to create a hermetic, rugged, stable, and safe stack, which is the urgent

* Corresponding authors.
E-mail: L. Luo, luolinghong@tsinghua.org.cn;
L. Wang, wly8858@163.com

requirement of the planar-type IT-SOFCs [6].

The sealing materials must simultaneously meet several requirements as follows: gas tightness, electrically insulation, suitable viscosity and chemical inertness, thermal expansion coefficient (TEC) compatibility, and good adherence with other cell components [7]. Sealing materials can be classified in two categories: (1) compressive seals such as metallic or mica-based, (2) rigid seals such as glass, glass-ceramics [8]. Because glass and glass-ceramic sealants exhibit strong bonding to the interface, many studies have been dedicated to optimize the formulation of glass-ceramics to meet most of the requirements. Through adjusting the formulation of glass, the TEC of glass could be directly changed to effectively avoid the stress caused by the mismatch of TEC among the sealants and other cell components at high temperature. Due to high expansion value and adjustable thermal expansion performance, $BaO–CaO–Al_2O_3–B_2O_3–SiO_2$ (BCABS) sealing glass has taken much attention of the researchers [9–12]. However, during the heat treatment condition, the hexagonal celsian phase (TEC = 8.0×10^{-6} K^{-1}) in BCABS glass would be transformed into the monoclinic celsian phase (TEC = 2.3×10^{-6} K^{-1}), which would decrease the TEC of BCABS glass to result in serious cracks along the interface of bonded materials [13]. Ghosh *et al.* [14] reported that the addition of LaO in BCABS sealants could increase the viscosity of the glass, and then inhibit the glass crystallization at relatively high temperature. Lin *et al.* [15] indicated that through adjusting the formulation of glass, the self-healing of $BaO–Al_2O_3–SiO_2$ based glass could fill the cracks caused by the stress under the heat treatment condition.

As seen from the above studies, the two critical parameters for the long-term sealing ability of sealing glass are the thermal expansion coefficient and glass crystallization temperature. In order to obtain a suitable glass sealant, it is essential to elucidate the crystallization kinetics of glass during the heat treatment condition, which is a key subject for researching glass crystallization and then providing new opportunity for structure control by innovative design and processing techniques. In addition, Al_2O_3 is the most frequently used intermediate in sealing glass, but almost the only intermediate in $BaO–CaO–Al_2O_3–B_2O_3–SiO_2$ (BCABS) glass, which could regulate the thermal properties of the glass well. If Al^{3+} was 4-coordinated, it would participate into the glass network and enhance the structure symmetry of glass [16]. Dai *et al.* [17] observed that increasing the aluminum content from 0 to 30 wt% in the Al_2O_3-based compressive seals decreases the leakage rate and increases the thermal cycle stability. Wang *et al.* [18] investigated the viability of the seal and found that the sealing performance of the seal is significantly improved by increasing the Al_2O_3 content and the seal containing 50 wt% Al_2O_3 shows the best sealing performance among the studied compositions. However, the role and the related influence of Al_2O_3 on the structure and crystallization dynamics of sealing glass have been poorly investigated. The purpose of this article was to study the influence of Al_2O_3 addition on the thermal performance of BCABS glass from the aspect of the non-isothermal crystallization kinetics.

2 Experimental

The BCABS sealing glass was prepared based on preliminary preparation [19], and the raw compositions of A and B glass sealants with different Al_2O_3 additions are listed in Table 1.

The raw materials composed of SiO_2 (analysis reagent, AR), Al_2O_3 (AR), H_3BO_3 (AR), $BaCO_3$ (AR), Na_2CO_3 (AR), and $CaCO_3$ (AR), were wet-mixed and melted in the high temperature chamber furnace in air. The molten glass was quenched, and then re-milled in alcohol (AR) for 4 h in a planetary ball miller (QM-3SP2). One part of pulverized glass was subsequently subjected to prepare the glass slab for the determination of the TEC, the glass transition temperature (T_g), and softening temperature (T_s) by dilatometric measurements (Dilatometer 402E NETZSCH, heat rating: 10 K/min). Through pressing the powders containing the polyvinyl butyral (PVB) binders into strips by the laminating machine (769YP-15A), the strips were obtained with

Table 1 Component ration of A and B glass

Component	Mole ration of A glass (mol%)	Mole ration of B glass (mol%)
SiO_2	28.52	28.52
Al_2O_3	4.20	10.31
H_3BO_3	25.23	25.23
$BaCO_3$	28.46	28.46
$CaCO_3$	12.48	12.48
Na_2CO_3	1.10	1.10
Total	100	106.11

the dimensions of 5 mm × 5 mm × 20 mm. The dry-pressed rectangular glass strips were heat-treated at 1123 K for 30 min in a fast heating furnace, and then conducted through the operating condition at 1023 K for 0 and 100 h. After that, these samples were used for the thermal expansion testing. Other glass powders were heated in differential thermal reanalysis (DTA, STA449C comprehensive thermal analyzer in Netzsch, Germany) at four different heating rates. The heat of transformation and other essential physical quantities were obtained from the thermograms with the help of software. Furthermore, the X-ray diffraction (XRD, Bruker AXSD8-Advance) with Cu Kα radiation was used to identify the formed crystalline phases of the quenched glass after different heating treatments. These pellets were recorded by Fourier transform infrared (FTIR) spectra in the range of 1500 to 400 cm^{-1} using a Perkin Elmer-Spectrum BX with a spectral resolution of 1 cm^{-1}. Each test sample was mixed with KBr in an agate mortar and then pressed into 13 mm diameter pellets.

The half-cell consisted of 8 mol% yttrium-stabilized zirconia (8YSZ) as the electrolyte and NiO/8YSZ as the anode. The above quenched BCABS glass powders with PVB binder were used to prepare plates, and then be pressed on the half-cell to obtain the glass/electrolyte–anode/glass samples with a sandwich structure. The sandwiched samples were firstly heated to the sealing temperature (1123 K) and maintained for 30 min, and then soaked at the operating temperature (1023 K) for 100 h. The microstructure of the interface between the glass layer and anode/electrolyte layer was obtained by using scanning electron microscopy (SEM, JSM-6700 F) techniques, which could be used to evaluate the adhesion of the glass on the electrolyte and anode in the half-cell.

3 Results and discussion

3. 1 FTIR investigation

FTIR transmission spectra of A and B glass with different Al_2O_3 addition at room temperature are shown in Fig. 1. The bands of 1393 and 1203 cm^{-1} are corresponding to B–O–B anti-symmetry stretching vibrations in $[BO_3]$ triangle and $[BO_4]$ tetrahedron, respectively [20]. The anti-symmetry stretching vibrations of the bridging oxygen bond Si–O–Si in $[SiO_4]$ tetrahedron and the non-bridging oxygen bond

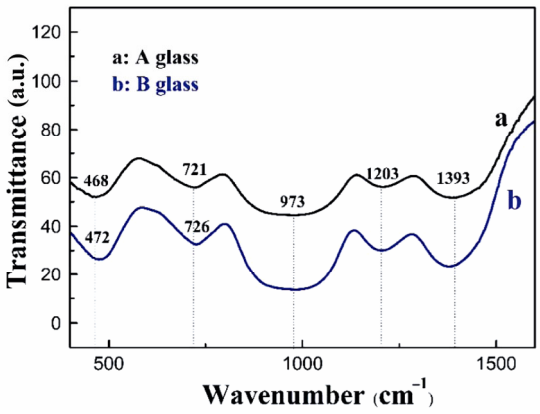

Fig. 1 FTIR spectra of A and B glass with different Al_2O_3 addition.

Si–O^- in silicate glass cause the absorption bands of 1040 and 950 cm^{-1}, respectively [21]. As shown in Fig. 1, the two absorption bands are combined together into one band of around 973 cm^{-1} in the FTIR spectra of A and B glass. The absorption band of 468 cm^{-1} is attributed to bending vibration of Si–O–Si/B–O–B linkage in A glass, which reveals on the band of 468 cm^{-1} in B glass. The absorption bands of 721 cm^{-1} in A glass and 726 cm^{-1} in B glass are corresponding to the stretching vibration of Si–O–Al [22], which verifies that the Al^{3+} ions exist in four-fold coordination in both A and B glass.

3. 2 Crystallization kinetic behavior by DTA

DTA has become a convenient and widely used tool for studying the kinetics of phase transformation, and the kinetic data on the phase transformation can be obtained from this technique in either non-isothermal or linear heating (scanning) mode [23]. Long-term thermal and chemical stability of sealing glass depends on the T_g and crystallization temperature (T_c) of glass during sealing [23]. To maintain the hermeticity of glass, T_g value should be below the operating temperature (1023 K) of IT-SOFC to relieve thermal stress and proceed self-healing of cracks, and T_c should be higher than 1023 K to avoid excessive glass flow. Different glass formulation can cause changes in T_g and T_s, which have great influence on the crystallization of glass. The crystallization of sealing glass is a great influence on adhesion between glass and other cell components during joining or operating period [24].

As shown in Fig. 2, the DTA thermograms of A and B glass powders are recorded at the heating rates of 5, 10, 15, and 35 K/min or 10, 15, 25, and 35 K/min,

respectively. There is a small endothermic peak attributed to the glass transition temperature range, and its lowest point refers to T_g. There is subsequently also an exothermic peak originating from the amorphous–crystalline transformation. The characteristic point of exothermic peak is corresponding to the maximum crystallization rate. The values of T_g and T_c for A and B glass are listed at different heating rates in Table 2.

The crystallization kinetics of the glass powders was studied using the formal theory of transformation kinetics as developed by Johnson and Mehl [25] and

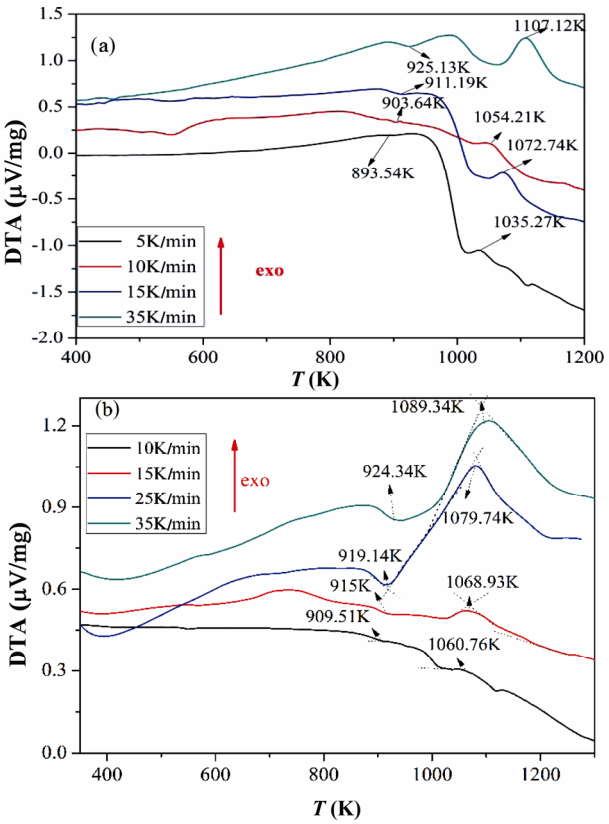

Fig. 2 DTA thermograms for (a) A and (b) B glass powders at different heating rates.

Table 2 Glass transition temperature (T_g) and the crystallization temperature (T_c) for A and B glass powders recorded at different heating rates

Sample	A (K/min)	T_g (K)	T_c (K)
A	5	893.54	1035.27
	10	903.64	1054.21
	15	911.19	1072.74
	35	925.13	1107.12
B	10	909.51	1060.76
	15	915	1068.93
	25	919.14	1079.74
	35	924.34	1089.34

Faleiros *et al.* [26] as shown below:

$$\ln\left(\frac{T_p^2}{\alpha}\right)=\frac{E_c}{RT_p}+k_1 \quad (1)$$

where α is the heating rate, k_1 is a constant, R is the gas constant. The relationship between $\ln\left(\frac{T_p^2}{\alpha}\right)$ versus $1000/T_p$ from the experimental data is plotted as shown in Fig. 3. The slope of this graph gives the activation energy of crystallization (E_c). The E_c of A and B glass could be calculated to be 233.89 and 406.03 kJ/mol, respectively. The result indicates that the B glass with the higher E_c is more difficult to crystallize, which could obtain more stable performance and wider practical application.

The Kissinger method is also valid for the glass transition and has often been used to calculate the activation energy for glass transition (E_t) by the following relation [27]:

$$\ln\left(\frac{T_g^2}{\alpha}\right)=\frac{E_t}{RT_g}+k_2 \quad (2)$$

Kissinger's formula [27] can also be used for the evaluation of the activation energy of the glass transition using the following formula:

$$\ln\left(\frac{1}{\alpha}\right)=\frac{E_t}{RT_g}+k_3 \quad (3)$$

The values of E_t calculated from the slopes of the plots (in Fig. 4 and Fig. 5) can be obtained according to formulas (2) and (3). The values E_t of A and B glass are 396.99 and 594.03 kJ/mol in Fig. 4, respectively. The slope in Fig. 5 shows the values of E_t of A and B glass are 411.93 and 609.22 kJ/mol, respectively. The activation energies of glass obtained in different methods have been summarized in Table 3. As shown in Table 3, the values calculated by the two methods are approximately equal, which verifies the effectiveness of the two methods. Ray [28] has reported that T_g is related to the density of covalent cross linking, number and strength of co-ordinate links formed between oxygen atoms and the cations, and the oxygen density of network, higher values of which correspond to higher T_g. The higher the activation energy for glass transition, the more stable the structure of the glass. In a word, the results show that the thermostability performance of B glass with more Al_2O_3 addition is higher than A glass.

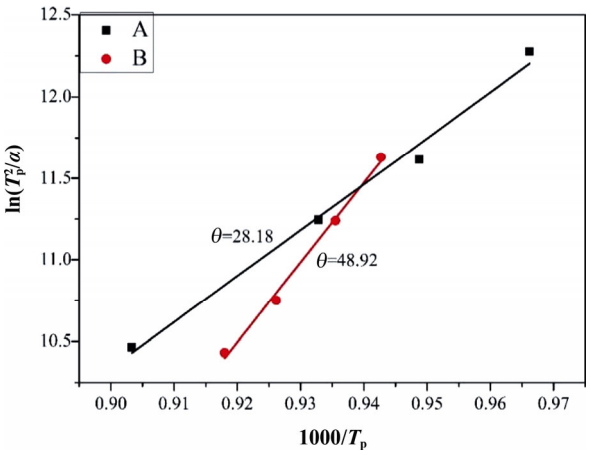

Fig. 3 $\ln(T_p^2/\alpha)$ versus $1000/T_p$ for A and B glass.

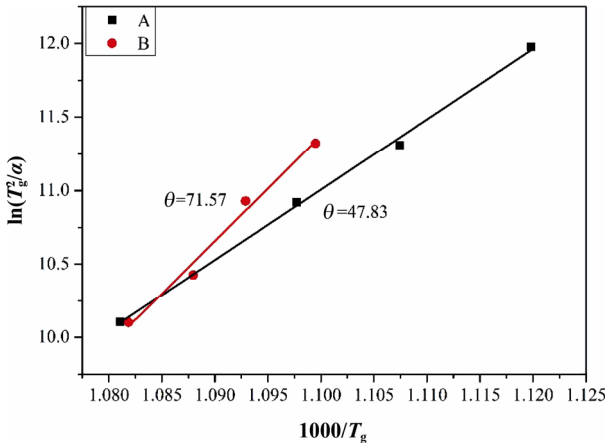

Fig. 4 $\ln(T_g^2/\alpha)$ versus $1000/T_g$ for A and B glass.

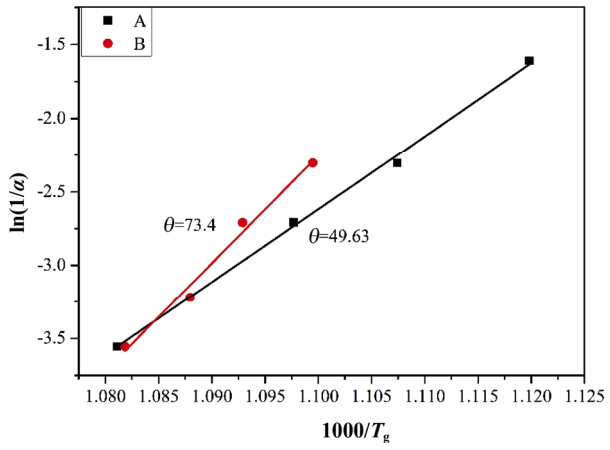

Fig. 5 $\ln(1/\alpha)$ versus $1000/T_g$ for A and B glass.

Table 3 Activation energies for the glass transition (E_t) and crystallization (E_c) of A and B glass

Sample	$\ln(T_p^2/\alpha)$ versus $1000/T_p$, E_c (kJ/mol)	$\ln(T_g^2/\alpha)$ versus $1000/T_g$, E_t (kJ/mol)	$\ln(1/\alpha)$ versus $1000/T_g$, E_t (kJ/mol)
A	233.89	396.99	411.93
B	406.03	594.03	609.22

3. 3 XRD for crystallization study

BaO is most likely modifying the silicate network, and then leads to form the hexagonal $BaAl_2Si_2O_8$ crystalline phase in the BCABS sealing glass. After the heat preservation at 1023 K for 0, 50, and 100 h, the XRD patterns of A and B glass show the evolution of crystalline phase in Fig. 6. With the increase of heating time, the peak of hexagonal celsian (22.37°) is gradually decreased, but that of the monoclinic celsian (28.65°) is increased. The result indicates that through the heat treatment, the hexagonal $BaAl_2Si_2O_8$ with the TEC of 8×10^{-6} K^{-1} is transformed into monoclinic $BaAl_2Si_2O_8$ (2.3×10^{-6} K^{-1}) [29]. In Fig. 6(a), after the heat treatment at 1023 K for 50 h, the intensity of the peaks of hexagonal $BaAl_2Si_2O_8$ phase is decreased, but that of monclinic $BaAl_2Si_2O_8$ phase is increased. A new phase ($Ba_2Ca(B_3O_6)_2$) at 29.17° is also appeared and unchanged with the increase of heat-treating time. However, by comparing Fig. 6(a) with Fig. 6(b), the obvious difference is that the curve in Fig. 6(b) is not changed after heating at 1023 K for 50 h, and the peak of the monclinic $BaAl_2Si_2O_8$ phase is weaker than that of Fig. 6(a) after heating at 1023 K for 100 h. There are small humps in the XRD patterns as Fig. 6(a) and Fig. 6(b) show, which indicates that the amorphous content in glass is still present. This amorphous content is consumed by crystalline phase $BaAl_2Si_2O_8$ and $Ba_2Ca(B_3O_6)_2$. The above results show that through the same heat treatment, the crystalline transformation rate of A glass is faster than that of B glass, and then determin that adding Al_2O_3 could effectively delay the transformation of crystalline phase in glass, which is consistent with the analysis results of the activation energy of the glass.

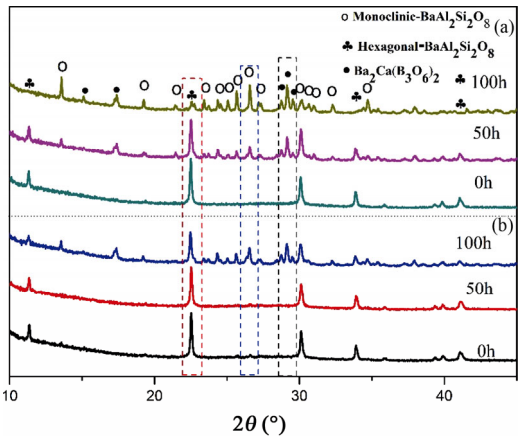

Fig. 6 XRD patterns of (a) A glass heat treated at 1023 K for 0, 50, and 100 h, and (b) B glass heat treated at 1023 K for 0, 50, and 100 h.

3. 4 Dilatometry measurements

To achieve the suitable sealing glass for IT-SOFCs, the TEC of the glass materials as the main criterion must be in the range of 9×10^{-6} to 12×10^{-6} K^{-1} under working temperature [30–32]. The measured linear TECs of the two kinds of glass are shown in Fig. 7, which could determine that the glass transition points are 858 and 834 K for A and B glass, respectively. The softening points for two kinds of glass are 911 and 1035 K for A and B glass, respectively. The results show the TECs of A and B glass are approximately equal and the values are $(10.5\pm0.2)\times10^{-6}$ K^{-1} before the heat preservation under rigid conditions. After the heat treatment at 1023 K for 100 h, the TEC value of A glass at 1023 K for 100 h is 8.2×10^{-6} K^{-1}, lower than 10.02×10^{-6} K^{-1} of B glass. It means that the crystal transformation rate in the A glass is faster than that of B glass, which is corresponding to the results of E_c. This phenomenon shows that the alumina could effectively increase the softening temperature of glass, which also indicates that B glass with more Al_2O_3 addition is more suitable for sealing at high temperature condition.

3. 5 Interfacial microstructures

In order to further verify the better sealing performance of B glass than that of A glass, the cross-sectional morphology of two kinds of glass after heat treatment at 1123 K for 30 min followed by soaking at 1023 K for 100 h were characterized by SEM testing. Figures 8(a) and 8(c) are SEM images with a magnification of

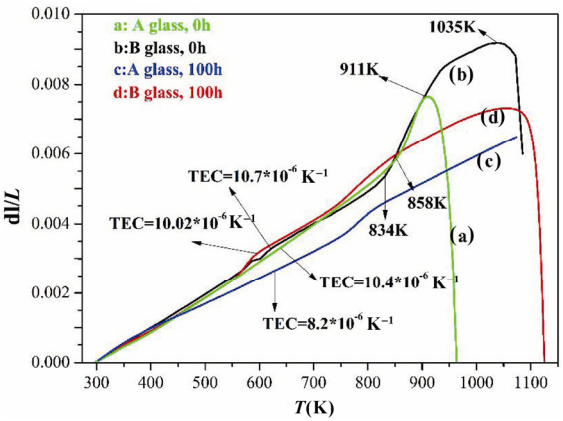

Fig. 7 Thermal expansion curves of glass after different heat treatment: (a) A glass at 1023 K for 0 h; (b) B glass at 1023 K for 0 h; (c) A glass at 1023 K for 100 h; (d) B glass at 1023 K for 100 h.

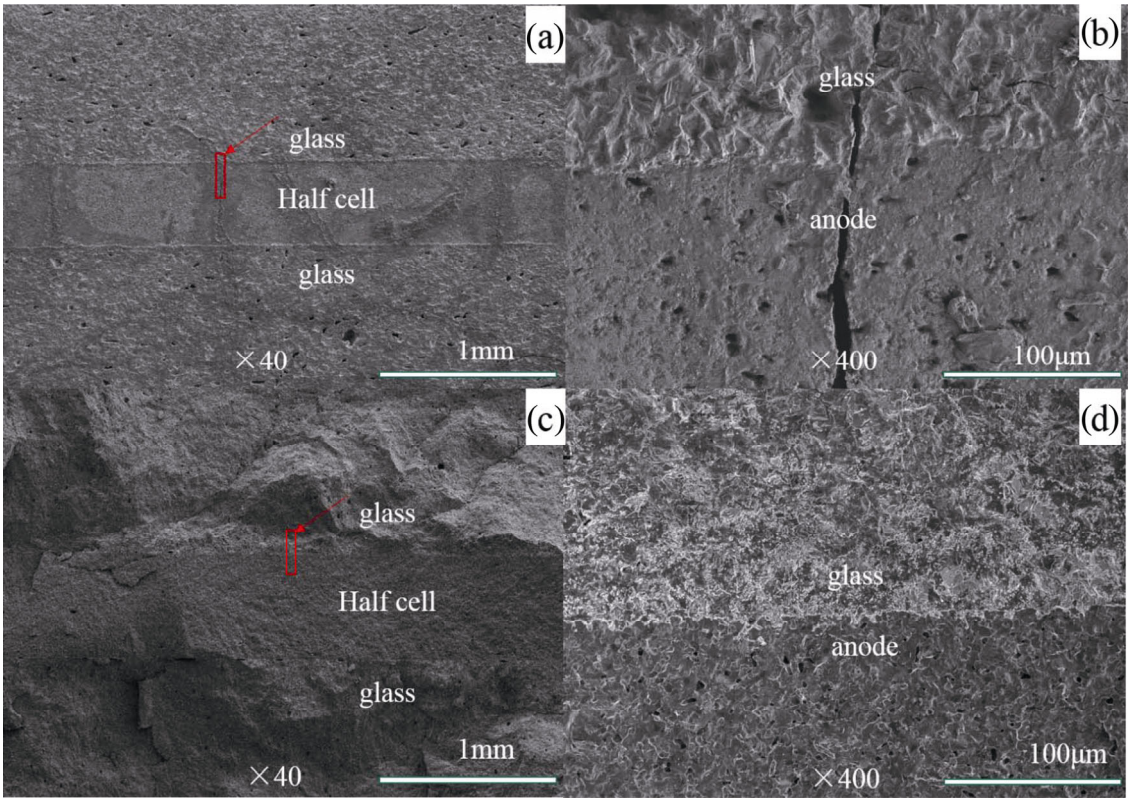

Fig. 8 Cross-sectional SEM images of sealing interface between glass and half-cell after the heat treatment at 1123 K for 30 min, followed by soaking at 1023 K for 100 h: (a) A glass/half-cell/A glass at 40× magnification; (b) A glass/anode at 400× magnification; (c) B glass/half-cell/B glass at 40× magnification; (d) B glass/anode at 400× magnification.

40 that show the sealing situation of A and B glass, respectively. Both the upper layer and the lower layer are the glass, and the middle layer is half-cell. As shown in Figs. 8(a) and 8(c), there are several cracks through the half-cell and A glass, but no cracks through the half-cell and B glass, which indicates that A glass has worse sealing performance than B glass during the long-term heat treatment. Figures 8(b) and 8(d) with a magnification of 400 are separately corresponding to the red rectangular area marked in Fig. 8(a) and Fig. 8(c). In Fig. 8(b), it could be seen that there is a clear crack through the anode and glass, which is due to the mismatch of TEC between the glass and the anode caused by the high-temperature cycling in Fig. 7. In Fig. 8(d), although the glass has been sintered relatively dense, there are still some closed pores filled in the glass region in Fig. 8(c). The appearance of closed porosity usually does not result in the enhancement of leak rate [33]. Therefore, this phenomenon shows that B glass could adhere well to half-cell and there are no cracks in the interface after 100 h heat treatment at 1073 K, which indicates that B glass is more suitable than A glass for IT-SOFCs sealing.

4 Conclusions

In this paper, the effects of Al_2O_3 addition on the thermal stability of BCABS glass were studied from the aspect of the crystallization kinetics. The FTIR spectra of glass with different Al_2O_3 content showed Al^{3+} ion is 4-coordinated and participated as network forming. XRD patterns verified that more Al_2O_3 content could decrease the formation of the monoclinic $BaAl_2Si_2O_8$ and $Ba_2Ca(B_3O_6)_2$ crystalline phase during the heat treatment at 1023 K for 100 h. Both of the activation energy for the glass transition and crystallization were increased, which effectively suppressed the crystallization ability of B glass with higher Al_2O_3 content under the heat treatment. The TEC of B glass was merely changed from $(10.5\pm0.2)\times10^{-6}$ to 10.02×10^{-6} K^{-1} through the high-temperature process. The sealing performance of glass by SEM testing further confirmed that B glass with more Al_2O_3 addition could adhere well to half-cell with no cracks in the interface after heat treatment, which is more beneficial for IT-SOFCs applications than A glass.

Acknowledgements

This study was financially supported by the research project of National Natural Science Foundation of China (Grant Nos. 51662015 and 51462011).

References

[1] Yang Z, Xia G, Meinhardt KD, *et al.* Chemical stability of glass seal interfaces in intermediate temperature solid oxide fuel cells. *J Mater Eng Perform* 2004, **13**: 327–334.

[2] Lim T-H, Park J-L, Lee S-B, *et al.* Fabrication and operation of a 1 kW class anode-supported flat tubular SOFC stack. *Int J Hydrogen Energ* 2010, **35**: 9687–9692.

[3] Bansal NP, Gamble EA. Crystallization kinetics of a solid oxide fuel cell seal glass by differential thermal analysis. *J Power Sources* 2005, **147**: 107–115.

[4] Lara C, Pascual MJ, Durán A. Glass-forming ability, sinterability and thermal properties in the systems $RO–BaO–SiO_2$ (R = Mg, Zn). *J Non-Cryst Solids* 2004, **348**: 149–155.

[5] Barelli L, Bidini G, Cinti G, *et al*. SOFC stack coupled with dry reforming. *Appl Energ* 2017, **192**: 498–507.

[6] Zhang W, Yan D, Duan J, *et al.* Development of Al_2O_3/glass-based multi-layer composite seals for planar intermediate-temperature solid oxide fuel cells. *Int J Hydrogen Energ* 2013, **38**: 15371–15378.

[7] Nguyen X-V, Chang C-T, Jung G-B, *et al*. Study of sealants for SOFC. *Int J Hydrogen Energ* 2016, **41**: 21812–21819.

[8] Lessing PA. A review of sealing technologies applicable to solid oxide electrolysis cells. *J Mater Sci* 2007, **42**: 3465–3476.

[9] Khedim H, Nonnet H, Méar FO. Development and characterization of glass-ceramic sealants in the ($CaO–Al_2O_3–SiO_2–B_2O_3$) system for solid oxide electrolyzer cells. *J Power Sources* 2012, **216**: 227–236.

[10] Smeacetto F, Chrysanthou A, Salvo M, *et al.* Performance and testing of glass-ceramic sealant used to join anode-supported-electrolyte to Crofer22APU in planar solid oxide fuel cells. *J Power Sources* 2009, **190**: 402–407.

[11] Smeacetto F, Salvo M, Bytner FDD, *et al*. New glass and glass–ceramic sealants for planar solid oxide fuel cells. *J Eur Ceram Soc* 2010, **30**: 933–940.

[12] Jin T, Lu K. Compatibility between AISI441 alloy interconnect and representative seal glasses in solid oxide fuel/electrolyzer cells. *J Power Sources* 2010, **195**: 4853–4864.

[13] Fu Y-P, Chang C-C, Lin C-H, *et al.* Solid-state synthesis of ceramics in the $BaO–SrO–Al_2O_3–SiO_2$ system. *Ceram Int* 2004, **30**: 41–45.

[14] Ghosh S, Das Sharma A, Kundu P, *et al.* Development and characterizations of $BaO–CaO–Al_2O_3–SiO_2$ glass–ceramic sealants for intermediate temperature solid oxide fuel cell application. *J Non-Cryst Solids* 2008, **354**: 4081–4088.

[15] Lin C-K, ChenT-T, Chyou Y-P, *et al.* Thermal stress analysis of a planar SOFC stack. *J Power Sources* 2007, **164**: 238–251.

[16] Mahapatra MK, Lu K, Reynonds Jr. WT. Thermophysical properties and devitrification of SrO–La_2O_3–Al_2O_3–B_2O_3–SiO_2-based glass sealant for solid oxide fuel/electrolyzer cells. *J Power Sources* 2008, **179**: 106–112.

[17] Dai Z, Pu J, Yan D, *et al*. Thermal cycle stability of Al_2O_3-based compressive seals for planar intermediate temperature solid oxide fuel cells. *Int J Hydrogen Energ* 2011, **36**: 3131–3137.

[18] Wang X, Yan D, Fang D, *et al.* Optimization of Al_2O_3–glass composite seals for planar intermediate-temperature solid oxide fuel cells. *J Power Sources* 2013, **226**: 127–133.

[19] Luo L, Lin Y, Huang Z, *et al.* Application of BaO–CaO–Al_2O_3–B_2O_3–SiO_2 glass–ceramic seals in large size planar IT-SOFC. *Ceram Int* 2015, **41**: 9239–9243.

[20] Goel A, Tulyaganov DU, Kharton VV, *et al*. The effect of Cr_2O_3 addition on crystallization and properties of La_2O_3-containing diopside glass-ceramics. *Acta Mater* 2008, **56**: 3065–3076.

[21] Kaky KM, Lakshminarayana G, Baki SO, *et al.* Structural, thermal, and optical analysis of zinc boron-aluminosilicate glasses containing different alkali and alkaline modifier ions. *J Non-Cryst Solids* 2017, **456**: 55–63.

[22] Kumar V, Rupali, Pandey OP, *et al.* Thermal and crystallization kinetics of yttrium and lanthanum calcium silicate glass sealants for solid oxide fuel cells. *Int J Hydrogen Energ* 2011, **36**: 14971–14976.

[23] Mahapatra MK, Lu K. Glass-based seals for solid oxide fuel and electrolyzer cells—A review. *Mat Sci Eng R* 2010, **67**: 65–85.

[24] Goel A, Shaaban ER, Melo FCL, *et al*. Non-isothermal crystallization kinetic studies on MgO–Al_2O_3–SiO_2–TiO_2 glass. *J Non-Cryst Solids* 2007, **353**: 2383–2391.

[25] Johnson WA, Mehl RF. Reaction kinetics in processes of nucleation and growth. *Transactions of the American Institute of Mining & Metallurgical Engineers* 1939, **135**: 416–430.

[26] Faleiros AC, Rabelo TN, Thim GP, *et al.* Kinetics of phase change. *Mat Res* 2000, **3**: 1103–1112.

[27] Kissinger HE. Reaction kinetics in differential thermal analysis. *Anal Chem* 1957, **29**: 1702–1706.

[28] Ray NH. Composition—property relationships in ionorganic oxide glasses. *J Non-Cryst Solids* 1974, **15**: 423–434.

[29] Lu Y-F, Du Y-G, Xiao J-Y, *et al.* Effect of ZrO_2 on crystallization and phase transformation in low-temperature processed BaO–Al_2O_3–SiO_2 glass-ceramics. *J Inorg Mater* 2008, **23**: 159–164.

[30] Lin C-K, Lin K-L, Yeh J-H, *et al*. Creep rupture of the joint of a solid oxide fuel cell glass–ceramic sealant with metallic interconnect. *J Power Sources* 2014, **245**: 787–795.

[31] Goel A, Tulyaganov DU, Kharton VV, *et al.* Electrical behavior of aluminosilicate glass-ceramic sealants and their interaction with metallic solid oxide fuel cell interconnects. *J Power Sources* 2010, **195**: 522–526.

[32] Eichler K, Solow G, Otschik P, *et al.* BAS ($BaO{\cdot}Al_2O_3{\cdot}SiO_2$)-glasses for high temperature applications. *J Eur Ceram Soc* 1999, **19**: 1101–1104.

[33] Karamanov A, Arrizza L, Matekovits I, *et al.* Properties of sintered glass-ceramics in the diopside–albite system. *Ceram Int* 2004, **30**: 2129–2135.

Open Access The articles published in this journal are distributed under the terms of the Creative Commons Attribution 4.0 International License (http://creativecommons.org/licenses/by/4.0/), which permits unrestricted use, distribution, and reproduction in any medium, provided you give appropriate credit to the original author(s) and the source, provide a link to the Creative Commons license, and indicate if changes were made.